An Adaptive Dynamic Reference Control for Power Converters in a Microgrid

Jayan, Vijesh; Mohammad Ghias, Amer Mohammad Yusuf; Guerrero, Josep M.; Merabet, Adel

Published in:
IEEE Transactions on Power Electronics

DOI (link to publication from Publisher):
10.1109/TPEL.2022.3158060

Publication date:
2022

Document Version
Accepted author manuscript, peer reviewed version

An adaptive dynamic reference control for power converters in a microgrid

Jayan, Vijesh; Amer Mohammad Yusuf Mohammad Ghias; Guerrero, Josep M.; Merabet, Adel

2022

Jayan, V., Amer Mohammad Yusuf Mohammad Ghias, Guerrero, J. M. & Merabet, A. (2022). An adaptive dynamic reference control for power converters in a microgrid. IEEE Transactions On Power Electronics, 37(8), 9164-9174. https://dx.doi.org/10.1109/TPEL.2022.3158060

https://hdl.handle.net/10356/157226

https://doi.org/10.1109/TPEL.2022.3158060

An Adaptive Dynamic Reference Control for Power Converters in a Microgrid

Vijesh Jayan, *Student Member, IEEE,* Amer M. Y. M. Ghias, *Senior Member, IEEE,* Josep M. Guerrero, *Fellow, IEEE,* and Adel Merabet, *Senior Member, IEEE*

***Abstract*—This paper proposes an adaptive dynamic reference control for power converters in a microgrid. Conventionally, two separate controllers are required to control the input current and the dc bus voltage. The proposed adaptive dynamic reference control eliminates the need for an additional controller by utilizing a simple discrete-time model to generate appropriate input current reference for the dc bus voltage regulation. The proposed technique is easy to design and guarantees a dynamic convergence of the dc bus voltage to its nominal reference even during non-idealities in the system, such as model parameter uncertainties, sensor imperfections, and unmodelled dynamics. A simple design procedure of the control parameters for the desired converter response is also provided based on a theoretical analysis. Unlike traditional linear controllers, the control parameter design of the proposed model is independent of the converter's operating point. Finally, the performance of the proposed technique is validated experimentally by using a finite control set model predictive control of a typical grid-connected application and is compared with both conventional dynamic reference control and traditional linear controller.**

***Index Terms*—Voltage control, Power control, Predictive control.**

I. Introduction

Recently the power converters have become a proven technology for integrating energy sources, storage devices, and critical loads into microgrids. Thus, developing an effective control technique for the converters in microgrids has become an area of interest. The classical linear controllers are widely used to control the converters in microgrids [1]–[5]. In general, two control loops based on the linear controller were used to control the voltage and current. The voltage control loop generated a current reference to compensate for the dc bus voltage, while the current control loop applied appropriate switching signals to the converter. These controllers were designed through proper tuning of their gain parameters to ensure a stable operation. However, such gains were obtained for a specific operating point and will not guarantee desired dynamic response for a wider operating range. Furthermore, the cascaded configuration of linear controllers not only increased system complexity but also required a proper tunning procedure to obtain appropriate controller gains for both voltage and current control loops.

Another notable control technique is the finite control set model predictive control (FCS-MPC) [6]. Unlike linear controllers, the FCS-MPC is easy to implement and possesses a faster dynamic response during any disturbance in the system. Also, the FCS-MPC easily incorporates system non-linearities and can attain multiple control objectives by simply incorporating the control variables into a cost function through weighting factors. The FCS-MPC implementation of the converter as an active front-end (AFE) rectifier [7], active power filter [8], and grid-connected with LCL filter [9] were reported in the literature. The current control loop in these papers was implemented by the FCS-MPC, which provided the optimum switching signals to the converter. However, the current reference was generated by a voltage control loop based on the linear controller. Due to the variable switching behavior of the converter caused by the FCS-MPC, obtaining appropriate controller gains for the linear controller becomes challenging. An improper selection of the gain parameters can affect the overall system performance and stability.

The problem mentioned above was solved by introducing a dynamic reference (DR) model [10]. Such a model generates appropriate current reference based on the dc bus voltage error without requiring an additional control loop. The FCS-MPC implementation with the DR model was reported for various applications, namely, grid-connected [11], [12], dc microgrid [13]–[16], hybrid ac/dc microgrid [17]–[20] etc. In these papers, the model utilized a single parameter N to control the dc bus voltage by generating appropriate power/current reference for FCS-MPC. However, the dc bus voltage failed to converge to its nominal reference during system parameter variations and model uncertainties. As a result, a significant steady-state error prevails in the dc bus voltage that can compromise the operation of its connected loads. Also, the desirable range of N that can be used in the model and its theoretical analysis were not provided in these papers. Another notable drawback is that compared to the conventional approach, the model required an additional current sensor at the dc side to estimate the dc load parameter. This will increase the overall system cost and is not attractive for the industry. A similar type of DR control, so-called dynamic evolution control, was presented in [21] and [22] for a hybrid energy storage system. The voltage was controlled by an exponential error function, where three parameters

This work was supported by the School of Electrical and Electronic Engineering at Nanyang Technological University, Ministry of Education, Singapore, under Grant AcRF TIER 1-2018-T1-002-109 (RG 171/18). *(Corresponding authors: Vijesh Jayan and Amer M. Y. M. Ghias).*

Vijesh Jayan and Amer M. Y. M. Ghias are with the School of Electrical and Electronic Engineering, Nanyang Technological University, Singapore 639798, Singapore (e-mail: vijeshja001@e.ntu.edu.sg; amer.ghias@ntu.edu.sg).

Josep M. Guerrero is with the Department of Energy Technology, Aalborg University, DK-9220 Aalborg, Denmark (email: joz@et.aau.dk).

Adel Merabet is with the Division of Engineering, Saint Mary's University, Halifax, NS B3H 3C3 Canada (email: adel.merabet@smu.ca).

determined its characteristics. These parameters were required to be tuned based on a desired transient response. However, detailed procedures for obtaining these parameters were not provided. Also, an improper selection of these parameters can cause overshoots in the system variables that can drastically affect the performance. An adaptive reference model predictive control (ARMPC) for a single-phase inverter was proposed in [23]. The ARMPC was based on the traditional FCS-MPC algorithm with a trajectory control theory that eliminated the steady-state error during a model parameter uncertainty. However, the implementation of ARMPC was complicated and required huge computations to identify the optimum switching state that eradicated the steady-state error. Another approach for the steady-state error elimination during a model parameter variation was to incorporate the past error of the control variable into the cost function of FCS-MPC [24]. However, such implementation required a variable weighting factor and an additional algorithm to determine its value during the operation.

Therefore, an adaptive dynamic reference (ADR) model is proposed in this paper that is easy to design and integrate into any power converter topology and microgrid applications. Following are the contributions overlaid in this paper:

1) The proposed ADR model eliminates the steady-state error in the dc bus voltage and guarantees the desired dynamic convergence to its nominal reference even during model parameter variation, unmodelled dynamics, and sensor imperfections.
2) The proposed technique is easy to implement as it does not require an accurate model with all dynamics incorporated and/or additional load current sensor at the dc side.
3) A theoretical analysis of the proposed ADR model is developed, and a simple three-step design procedure is overlaid to obtain the optimal control parameters for the desired converter response. Unlike traditional PI controllers, the design of the ADR model is independent of the converter's operating point.
4) The proposed model is verified experimentally on a typical grid-connected converter using FCS-MPC under different scenarios, and its performance is compared with the DR model [10] and traditional PI controller.

The paper is organized as follows: Section II describes the FCS-MPC that is used to validate the performance of the DR models. Section III discusses the limitation of conventional DR model. Section IV proposes the ADR model with its operation and design equations. Section V discusses the implementation of traditional PI controller and its comparison with proposed ADR model. Section VI validates the proposed method experimentally under different case studies followed by the conclusions.

II. FCS-MPC

A block diagram of FCS-MPC implementation for a typical grid-connected converter is shown in Fig. 1. The FCS-MPC is designed to control the grid current. Thus, a discrete-time prediction model of the grid current $\mathbf{i} = [i_\alpha \; i_\beta]^T$ is developed,

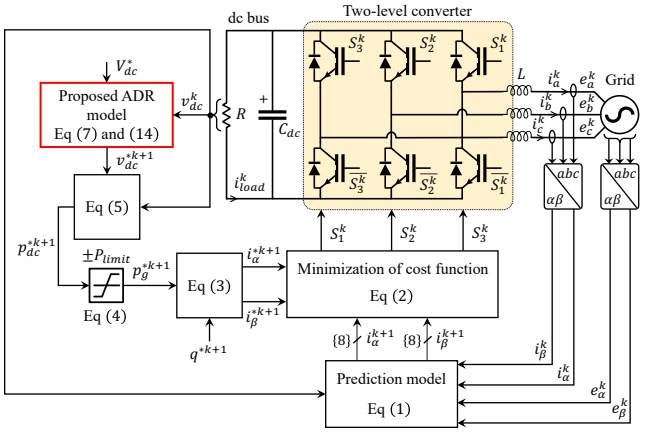

Fig. 1. The block diagram of FCS-MPC implementation for a grid-connected two-level converter with the proposed ADR model.

which can be expressed in terms of the converter's switching signals S_1, S_2, S_3 and grid voltage $\mathbf{e} = [e_\alpha \; e_\beta]^T$ as

$$\mathbf{i}^{k+1} = \mathbf{i}^k + \frac{T_s}{L}\left(\sqrt{\frac{2}{3}}\begin{bmatrix}1 & -\frac{1}{2} & -\frac{1}{2}\\ 0 & \frac{\sqrt{3}}{2} & -\frac{\sqrt{3}}{2}\end{bmatrix}\begin{bmatrix}S_1^k\\ S_2^k\\ S_3^k\end{bmatrix} v_{dc}^k - \mathbf{e}^k\right), \tag{1}$$

where v_{dc}^k is dc bus voltage measured at time instant k, and T_s is the controller sampling period. The detailed procedure of deriving (1) can be found in [25]. The FCS-MPC obtains the optimum S_1, S_2, S_3 from a finite set of eight possibilities that minimizes a cost function based on the grid current. This paper considers a quadratic cost function J^k, which is expressed as

$$J^k = \left[\mathbf{i}^{*k+1} - \mathbf{i}^{k+1}\right]^T \left[\mathbf{i}^{*k+1} - \mathbf{i}^{k+1}\right], \tag{2}$$

where $\mathbf{i^{*k+1}} = [i_\alpha^{*k+1} \; i_\beta^{*k+1}]^T$ is the grid current reference, which is generated by the instantaneous power theory [26] as

$$\begin{bmatrix} i_\alpha^{*k+1}\\ i_\beta^{*k+1}\end{bmatrix} = \frac{1}{(e_\alpha^k)^2 + (e_\beta^k)^2}\begin{bmatrix} e_\alpha^k & e_\beta^k\\ e_\beta^k & -e_\alpha^k\end{bmatrix}\begin{bmatrix}-p_g^{*k+1}\\ q^{*k+1}\end{bmatrix}, \tag{3}$$

where p_g^* is the grid active power reference, and q^* is the grid reactive power reference. Note that the p_g^* is the power required to regulate the dc bus capacitor C_{dc} to its nominal voltage reference V_{dc}^*. Thus, the discrete-time equation of the p_g^* in terms of dc bus power reference p_{dc}^* can be expressed as

$$p_g^{*k+1} = \begin{cases} -P_{limit}, & \text{if } p_{dc}^{*k+1} < -P_{limit}\\ +P_{limit}, & \text{if } p_{dc}^{*k+1} > +P_{limit}\\ p_{dc}^{*k+1}, & \text{otherwise}\end{cases}, \text{ where} \tag{4}$$

$$p_{dc}^{*k+1} = v_{dc}^{*k+1} i_{dc}^{*k+1} \text{ and } i_{dc}^{*k+1} = \frac{C_{dc}}{T_s}\left(v_{dc}^{*k+1} - v_{dc}^k\right). \tag{5}$$

The $\pm P_{limit}$ ensures a safe converter operation by clamping the $\mathbf{i}^*$ generation (3) to maximum permissible grid current limit I_{limit}. Observe that the v_{dc}^{*k+1} in (5) is the dynamic voltage reference generated by the DR model to regulate the C_{dc} to V_{dc}^* (see Fig. 1). The upcoming section elaborates on the discrete-time equation of v_{dc}^* in a conventional DR model and its limitations. Note that the q^* is the reactive power required

to control the grid power factor. The grid operates in unity power factor (UPF) when the $q^* = 0$.

III. Conventional DR Model

A. Discrete-time equation

The discrete-time equation of the conventional DR model [10] is given as

$$v_{dc}^{*k+1} = v_{dc}^{k} + \frac{V_{dc}^{*} - v_{dc}^{k}}{N_R}, \tag{6}$$

where N_R is the parameter that controls the convergence of v_{dc}^* to V_{dc}^*. The time taken for the v_{dc}^* to reach V_{dc}^* is proportional to the magnitude of N_R. Thus, the DR model with a smaller N_R magnitude possesses a faster convergence of v_{dc}^* to V_{dc}^*. However, the usage of a smaller N_R value can distort the grid current during the steady-state operation. On substituting (6) to (5), the expression of p_{dc}^* is observed to have a direct dependency on the factor $\frac{C_{dc}}{T_s N_R}$ and the dc bus voltage error $(V_{dc}^* - v_{dc}^k)$. The DR model with a small N_R magnitude amplifies the $(V_{dc}^* - v_{dc}^k)$ to generate an undesirable fluctuating p_{dc}^* during the steady-state. This results in the distortion of the i_α^* and i_β^* (3). Hence, the magnitude of N_R is required to be greater than $\frac{C_{dc}}{T_s}$ ratio to ensure undistorted i_a, i_b, and i_c throughout the operation.

B. Limitations

Despite being a simple model, the conventional DR model fails to converge v_{dc}^* to V_{dc}^* during non-idealities in the system, such as model parameter uncertainties, sensor imperfections, and unmodelled dynamics. The step-response of the DR model with $N_R = 500$ and $N_R = 800$ for a non-ideal system is shown in Fig. 2. During a non-ideality in the system, the voltage attained at $k+1$ time instant will be different from the computed voltage reference (i.e, $v_{dc}^{k+1} \neq v_{dc}^{*k+1}$). This resulting voltage difference for a non-ideal system is demonstrated as δv_{dc} in the zoomed view of Fig. 2. The presence of δv_{dc} in the system introduces a steady-state error in the v_{dc}.

The v_{dc}^* is observed to settle at a value less than V_{dc}^* with a voltage offset $v_{off} = N_R \delta v_{dc}$. Even though the magnitude of δv_{dc} is of the order 10^{-4}, its effect on v_{dc}^* depends on the magnitude of N_R. The v_{off} is zero irrespective of N_R only when the system is ideal ($\delta v_{dc} = 0$). Nevertheless, for a non-ideal system ($\delta v_{dc} > 0$), the v_{off} increases proportionally to the magnitude of N_R. This suggests that the v_{off} can be minimized by reducing the value of N_R. However, reduction in the magnitude of N_R beyond $\frac{C_{dc}}{T_s}$ ratio can distort the i_a, i_b, and i_c, as discussed in Section III-A. Thus, the conventional DR model finds it impossible to eradicate the v_{off} from the v_{dc}^*. Hence, an enhanced DR model is proposed in this paper that eliminates the v_{off} and guarantees a dynamic convergence of the v_{dc}^* to V_{dc}^* even during system non-idealities.

IV. The Proposed ADR Model

The discrete-time equation of the proposed ADR model is defined as

$$v_{dc}^{*k+1} = v_{dc}^{k} + \frac{V_{dc}^{*} - v_{dc}^{k}}{N_R} + \frac{A^k}{N_L}. \tag{7}$$

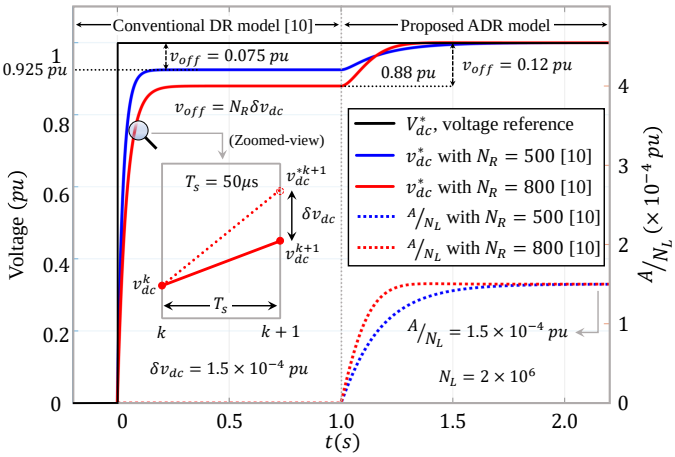

Fig. 2. Evolution of v_{dc}^* generated by the conventional DR model [10] and the proposed ADR model for a non-ideal system.

Compared to (6), (7) has $\frac{A^k}{N_L}$ as an additional term. The A^k is an accumulator, which performs a cumulative summation of the $V_{dc}^* - v_{dc}^k$ over time and the parameter N_L decides the rate at which the accumulated error is incorporated for v_{dc}^* generation. Fig. 2 demonstrates the role of $\frac{A}{N_L}$ in providing necessary corrections to v_{dc}^* for eliminating v_{off}. Observe that v_{off} is eliminated when $\frac{A}{N_L}$ approaches δv_{dc}. As a result, the proposed technique guarantees a smooth convergence of v_{dc}^* to V_{dc}^* for a non-ideal system.

A. Continuous-time model

To examine the effect of parameters N_R and N_L on v_{dc}^* generation, a continuous-time equation of (7) is derived. By considering $v_{dc}^k = v_{dc}^{*k}$, the resulting discrete-time equation of (7) can be written as

$$v_{dc}^{*k+1} = v_{dc}^{*k} + \frac{V_{dc}^{*} - v_{dc}^{*k}}{N_R} + \frac{\sum_{m=1}^{k} (V_{dc}^{*} - v_{dc}^{*m})}{N_L}. \tag{8}$$

Observe that A^k in (8) is expressed as the summation of the dc bus voltage error over time, as discussed previously. On setting $v_{dc}^{*k} = v_{dc}^*(t)$ and $V_{dc}^* = V_{dc}^*(t)$, (8) can be written as

$$\Delta v_{dc}^*(t) = \frac{V_{dc}^*(t) - v_{dc}^*(t)}{N_R} + \frac{1}{T_s} \int_{t=0}^{\infty} \frac{V_{dc}^*(t) - v_{dc}^*(t)}{N_L} dt. \tag{9}$$

Further dividing (9) by T_s and differentiating with respect to t, the continuous-time equation of the proposed ADR model is obtained as

$$\frac{d^2 v_{dc}^*(t)}{dt^2} + \frac{1}{N_R T_s} \frac{dv_{dc}^*(t)}{dt} + \frac{v_{dc}^*(t)}{N_L T_s^2} = \frac{1}{N_R T_s} \frac{dV_{dc}^*(t)}{dt} + \frac{V_{dc}^*(t)}{N_L T_s^2}. \tag{10}$$

Observe that the continuous-time equation expressed in (10) is a second-order system whose response is dependent on the values of N_R and N_L. Such a second-order model is prone to generate an oscillatory v_{dc}^* with significant overshoot during a step-response, as shown in Fig. 3a. Therefore, a proper

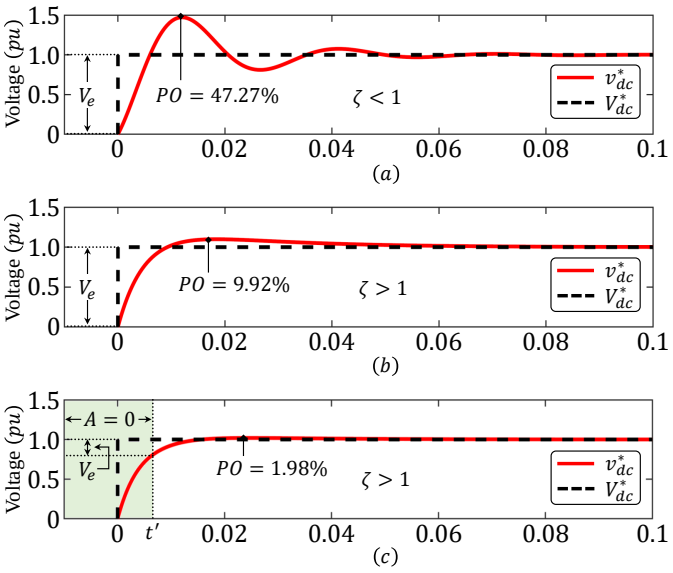

Fig. 3. Effect of step-response on the proposed ADR model with (a) $N_R = 800$, $N_L = 2 \times 10^5$, $V_e = V^*_{dc}$, (b) $N_R = 400$, $N_L = 10^6$, $V_e = V^*_{dc}$, and (c) $N_R = 400$, $N_L = 10^6$, $V_e = 0.2V^*_{dc}$.

selection of N_R and N_L is required to generate a desirable v^*_{dc} that is non-oscillatory and has minimal overshoot.

B. Effect of parameters on v^*_{dc} generation

In general, the degree of oscillation and magnitude of overshoot for a second-order system is quantified by the damping-ratio ζ and the natural frequency ω_n. The dependency of N_R and N_L on ζ and ω_n can be assessed by applying the Laplace transformation on (10). Thus, the proposed ADR model in s-domain can be expressed as

$$s^2 v^*_{dc}(s) - s v^*_{dc}(0) - \frac{dv^*_{dc}(0)}{dt} + \frac{s v^*_{dc}(s) - v^*_{dc}(0)}{N_R T_s} + \frac{v^*_{dc}(s)}{N_L T_s^2} = \frac{s V^*_{dc}(s) - V^*_{dc}(0)}{N_R T_s} + \frac{V^*_{dc}(s)}{N_L T_s^2}. \quad (11)$$

On substituting the initial conditions: $\frac{dv^*_{dc}(0)}{dt} = 0$, $v^*_{dc}(0) = 0$, $V^*_{dc}(0) = 0$ to (11), the $v^*_{dc}(s)$ can be expressed in terms of $V^*_{dc}(s)$ as

$$v^*_{dc}(s) = \frac{\frac{1}{N_R T_s} s + \frac{1}{N_L T_s^2}}{s^2 + \frac{1}{N_R T_s} s + \frac{1}{N_L T_s^2}} V^*_{dc}(s). \quad (12)$$

On comparing the denominator of (12) with the coefficients of a typical second-order characteristic equation [27], ζ and ω_n can be obtained in terms of N_R, N_L, and T_s as

$$\zeta = \frac{\sqrt{N_L}}{2N_R}, \text{ and } \omega_n = \frac{1}{T_s \sqrt{N_L}}. \quad (13)$$

The generation of v^*_{dc} during a step-response of (12) for different values of N_R and N_L are shown in Fig. 3. It is seen from Fig. 3a that the model with $N_R = 800$ and $N_L = 2 \times 10^5$ generates an oscillatory v^*_{dc} with significant overshoot. This is because the model is under-damped for $\zeta < 1$ (13). Therefore, values of N_R and N_L resulting in $\zeta < 1$ is not desirable. The step-response for a model with $\zeta > 1$ is shown in Fig. 3b. It is seen that the model possesses an over-damped response and generates a non-oscillatory v^*_{dc}. However, an overshoot persists in its response, which is not desirable. The overshoot is quenched by switching the order of the model, which is accomplished by adjusting the value of A^k as

$$A^k = \begin{cases} 0, & \text{if } V_e < |V^*_{dc} - v^k_{dc}| \\ A^{k-1} + V^*_{dc} - v^k_{dc}, & \text{if } V_e \geq |V^*_{dc} - v^k_{dc}| \end{cases}, \quad (14)$$

where V_e setting decides the value of A^k based on the dc bus voltage error $|V^*_{dc} - v^k_{dc}|$. The step-response of the model used in Fig. 3b with $V_e = 0.2V^*_{dc}$ is shown in Fig. 3c. Until time instant t', the $|V^*_{dc} - v^k_{dc}| > V_e$. As a result, $A = 0$ (14) and the model becomes a first-order system, where its response depends only on N_R (shaded region in Fig. 3c). At time instant t', the $|V^*_{dc} - v^k_{dc}| < V_e$ and the model becomes a second-order system. As a result, A begins to accumulate the $(V^*_{dc} - v^k_{dc})$ over time and incorporates it for v^*_{dc} generation through N_L. In doing so, the percentage overshoot PO in v^*_{dc} is found to reduce. Although the same values of N_R and N_L are used for the model shown in Fig. 3b, the PO in Fig. 3c is observed to reduce by a factor of 0.2. Therefore, the selection of V_e plays a crucial role in quenching the overshoots in the v^*_{dc} response. To examine the effect of V_e on PO, the expression for $v^*_{dc}(t)$ is derived by applying inverse Laplace transform on (11) with initial conditions: $\frac{dv^*_{dc}(0)}{dt} = 0$, $v^*_{dc}(0) = V^*_{dc} - V_e$, and $V^*_{dc}(0) = V^*_{dc} - V_e$. The resulting expression for $v^*_{dc}(t)$ is obtained as

$$v^*_{dc}(t) = \begin{cases} V^*_{dc} - V_e \left(\cos yt - \frac{x}{y} \sin yt \right) e^{-xt}, & \text{for } \zeta \neq 1 \\ V^*_{dc} - V_e \left(1 - xt\right) e^{-xt}, & \text{for } \zeta = 1 \end{cases}, \quad (15)$$

$$\text{where } x = \frac{0.5}{N_R T_s}, \text{ and } y = \frac{x}{\zeta} \sqrt{1 - \zeta^2}. \quad (16)$$

The stepwise procedure to obtain (15) can be found in Appendix A. The PO in $v^*_{dc}(t)$ with respect to V^*_{dc} is given as

$$PO = \frac{v^*_{dc}(t_m) - V^*_{dc}}{V^*_{dc}} \times 100, \quad (17)$$

where t_m is the time to reach the maximum overshoot, which is expressed as

$$t_m = \begin{cases} \frac{\pi}{y} + \frac{1}{y} \tan^{-1} \left(\frac{2xy}{x^2 - y^2} \right), & \text{for } \zeta < 1/\sqrt{2} \\ 4N_R T_s, & \text{for } \zeta = 1 \\ \frac{1}{y} \tan^{-1} \left(\frac{2xy}{x^2 - y^2} \right), & \text{for } \zeta \geq 1/\sqrt{2} \end{cases}. \quad (18)$$

The stepwise procedure to obtain (18) can be found in Appendix B. From (15), (17), and (18), the PO in v^*_{dc} can be obtained as

$$PO = 100 \frac{V_e}{V^*_{dc}} e^{-xt_m}. \quad (19)$$

The effect of V_e for different values of N_R and N_L is analyzed using (19) and is shown in Fig. 4. It is seen that the magnitude of PO increases as the values of N_R and N_L move from an over-damped region ($\zeta - 1 > 0$) to an under-damped region

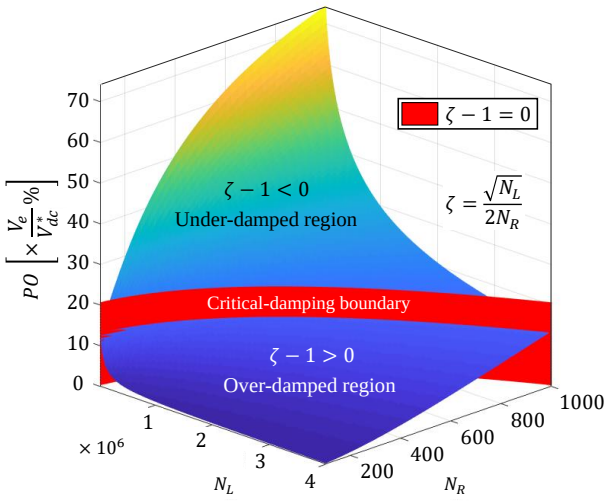

Fig. 4. Effect of N_R and N_L on PO in v_{dc}^*.

$(\zeta - 1 < 0)$. This concludes that the magnitude of PO is inversely proportional to ζ. Another notable aspect in (19) is that the magnitude of PO have a direct dependency on V_e. Thus, to reduce the PO in v_{dc}^* either a model with large ζ or small V_e can be selected.

C. Parameter design procedure

The optimum values of N_R, N_L, and V_e for the desired converter response are determined by adopting a simple three-step design procedure as follows:

1) Select parameter N_R such that its magnitude is greater than the $\frac{C_{dc}}{T_s}$ ratio.
2) Select parameter N_L such that the resulting ζ (13) based on the selected N_R is greater than 1. In other words, the selected N_R, N_L pair must belong to the over-damped region, as shown in Fig. 4.
3) Calculate V_e from (19) based on the selected N_R, N_L pair and desired PO limit.

Based on the values of C_{dc} and T_s given in Table I, $N_R = 200$, $N_L = 10^6$ $(\zeta = 2.5)$ is selected to guarantee a non-oscillatory v_{dc}^*, and $V_e = 0.1V_{dc}^*$ is chosen to limit the PO in v_{dc}^* to 0.32% (19).

V. Comparison with PI controller

The block diagram of a typical outer loop PI controller for dc bus voltage regulation is shown in Fig. 5. The PI controller generates p_{dc}^* based on the error in the dc bus voltage. The generated p_{dc}^* is limited by $\pm P_{limit}$ (4) and converted to desired grid current references i_α^*, i_β^* using (3), which is further sent to an inner loop current controller that operates on FCS-MPC as demonstrated in Fig. 1. The FCS-MPC applies optimum control action to attain p_{dc}^*, which subsequently regulates v_{dc} to V_{dc}^*. The transfer function of

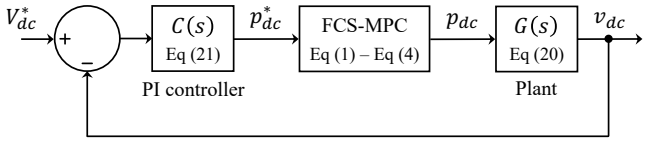

Fig. 5. Block diagram of a typical outer loop PI controller for dc bus voltage regulation.

the PI controller $C(s)$ and the plant $G(s)$ corresponding to the dc bus side can be expressed as

$$G(s) = \frac{R}{2V_{dc}^*\left(1 + \frac{RC_{dc}}{2}s\right)}, \text{ and} \tag{20}$$

$$C(s) = K_p + \frac{K_i}{s}, \tag{21}$$

where K_p and K_i are the gain parameters of the PI controller, which are tuned to accomplish a desired dc bus voltage response. Since the inner loop operates on FCS-MPC with a smaller T_s, let's set $p_{dc} = p_{dc}^*$. Thus, the closed-loop transfer function of the block diagram depicted in Fig. 5 can be obtained as

$$\frac{v_{dc}(s)}{V_{dc}^*(s)} = \frac{\frac{K_i}{C_{dc}V_{dc}^*}\left(1 + \frac{K_p}{K_i}s\right)}{s^2 + \frac{1}{C_{dc}V_{dc}^*}\left(K_p + \frac{2V_{dc}^*}{R}\right)s + \frac{K_i}{C_{dc}V_{dc}^*}}. \tag{22}$$

On comparing the denominator of (22) with the coefficients of a typical second-order characteristic equation [27], the ζ and ω_n can be obtained as

$$\zeta = \frac{K_pR + 2V_{dc}^*}{2R\sqrt{K_iC_{dc}V_{dc}^*}}, \text{ and } \omega_n = \sqrt{\frac{K_i}{C_{dc}V_{dc}^*}}. \tag{23}$$

The values of ζ and ω_n are selected based on a desired dc bus voltage response. The corresponding gain parameters K_p and K_i are calculated from (23) based on the selected ζ and ω_n values [8]. Observe from (23) that K_p and K_i is also dependent on R and V_{dc}^* values. This suggests that the PI controller guarantees the desired dc bus voltage response only when the converter operates at the values of R and V_{dc}^* that was considered for calculating K_p and K_i. Thus, the PI controller does not offer the desired dc bus voltage response when the converter undergoes a step-change to different R and/or V_{dc}^* values. On the other hand, the parameters N_R and N_L of the proposed ADR model are independent of the R and V_{dc}^* values (13). As a result, the designed ADR model, demonstrated in Section IV-C, exhibits the desired dc bus voltage response even when the converter step-changes to any values of R and V_{dc}^*. Furthermore, the PI controller requires an anti-windup scheme, such as back-calculation method, clamping method, etc. to prevent undesirable overshoot in the dc bus voltage. While the ADR model features parameter V_e, whose value is set easily using (19) to limit the overshoot in the dc bus voltage to a desirable value; thereby, eliminating the need for an anti-windup scheme.

VI. Experimental results

The proposed ADR model was validated using a low-power grid-connected converter. A picture of the experimental setup

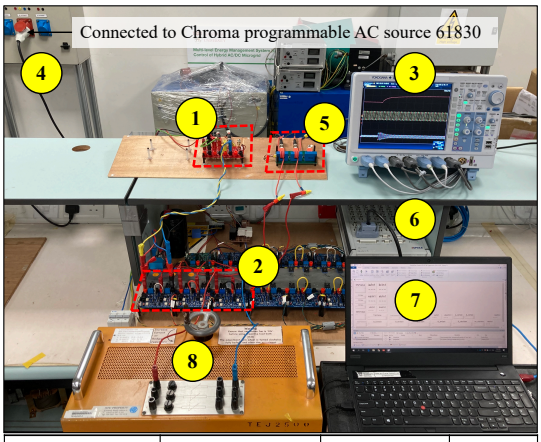

1. Voltage sensors $[e_a, e_b, v_{dc}]$	2. Three-phase two-level converter	3. Oscilloscope	4. Grid
5. Current sensors $[i_a, i_b]$	6. dSPACE MicroLabBox 1202	7. Host PC	8. dc load

Fig. 6. Picture of the experimental setup.

TABLE I
PARAMETERS FOR EXPERIMENTAL TEST

System and control parameters				
$\hat{E}$	f	L	C_{dc}	P_{limit}
30V	50Hz	6.3mH	2.2mF	225W
T_s	N_R	N_L	ζ	V_e
50μs	200	10^6	2.5	$0.1V_{dc}^*$
Load and reference parameters				
Case study	t(s)	$R(\Omega)$	V_{dc}^*(V)	q^*(VAR)
1	$0.1-0.5$	150	80	0
	$0.5-1.0$	150	120	0
2	$0.0-1.0$	150	100	0
	$1.0-3.0$	75	100	0
	$3.0-5.0$	75	100	100
3 4	$0.0-5.0$	75	100	0
5	$0.2-1.0$	100	100	0
	$1.0-2.0$	∞	100	0

is shown in Fig. 6. The three-phase two-level converter is built using six SiC MOSFETs G3R75MT12D with integrated gate driver boards, and the three-phase grid is emulated by a Chroma programmable AC source 61830. The converter is controlled using the FCS-MPC algorithm (see Fig. 1), programmed in MATLAB/Simulink, and implemented in dSPACE MicroLabBox 1202. The system and control parameters considered for the experimental validation are summarized in Table I. Different case studies evaluating the performance of the proposed ADR model and its comparison with the conventional DR model and traditional PI controller are demonstrated in the upcoming sub-sections.

A. *Case study* 1*: Step-response of* V_{dc}^*

The converter's performance with the proposed ADR model during a step-response of V_{dc}^* is shown in Fig. 7. In this study,

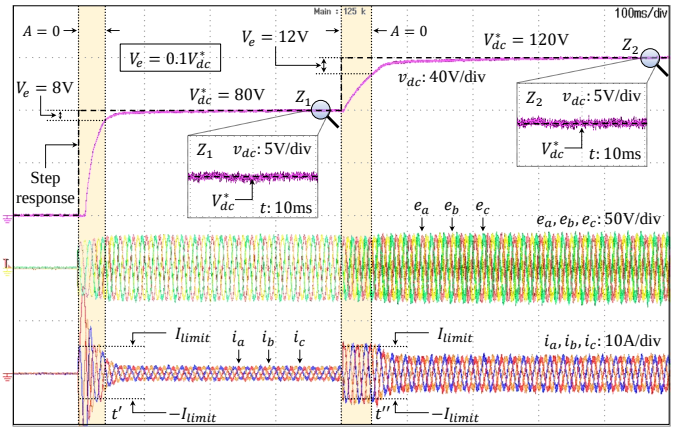

Fig. 7. Experimental result on the converter's performance with the proposed ADR model during a step-response of V_{dc}^*.

all the system variables are initialized to zero and q^* is set to 0VAR. At time instant $t = 100$ms, the converter is connected to the grid, and the controller is activated with $V_{dc}^* = 80$V. Observe that the $|V_{dc}^* - v_{dc}^k|$ at $t = 100$ms is greater than $V_e = 8$V ($V_e = 0.1V_{dc}^*$). As a result, $A = 0$ (see (14)), and the proposed ADR model operates as a first-order system that generates v_{dc}^* using N_R alone. After time instant t', the $|V_{dc}^* - v_{dc}^k|$ falls below 8V. Consequently, the proposed model switches to a second-order system, where N_R, N_L, and the accumulated dc bus voltage error A controls v_{dc}^* generation. It is seen that the v_{dc} exhibits a smooth trajectory and converges to 80V without introducing undesirable oscillation and overshoot in the system variables. At $t = 500$ms, the V_{dc}^* is increased to 120V. Observe that A is reset back to 0 as $|V_{dc}^* - v_{dc}^k| > 12$V, and the proposed ADR model becomes a first-order system. After t'', the model switches to a second-order system ($|V_{dc}^* - v_{dc}^k| < 12$V), which ensures a smooth convergence of v_{dc} to 120V. Note that during the transients, the peak of i_a, i_b, and i_c are limited to $I_{limit} = 5$A due to the P_{limit} setting (4).

B. *Case study* 2*: Step-response of load and reactive power*

The converter's performance with the proposed ADR model during a step-response of load and reactive power is shown in Fig. 8. In this study, the V_{dc}^* is set to 100V throughout the operation. Until $t = 1$s, the dc load resistance $R = 150\Omega$ and $q^* = 0$VAR. The grid operates in UPF as its three-phase voltage and current are in-phase (see zoomed view of Fig. 8). At $t = 1$s, the load undergoes a step-change to 75Ω. The proposed ADR model identifies the deviation in v_{dc} caused by the load-change and provides necessary adjustments to v_{dc}^* for its regulation. As a result, v_{dc} smoothly converges back to 100V and the grid continues operating at UPF. At $t = 3$s, the q^* undergoes a step-change to 100VAR. A phase difference of $\Delta\phi = 29.6°$ is observed between the three-phase voltage and current (see a zoomed view of Fig. 8). As a result, the grid operates at a power factor of 0.87. The v_{dc} is not affected during a step-change in q^* and continues regulating to 100V during the operation.

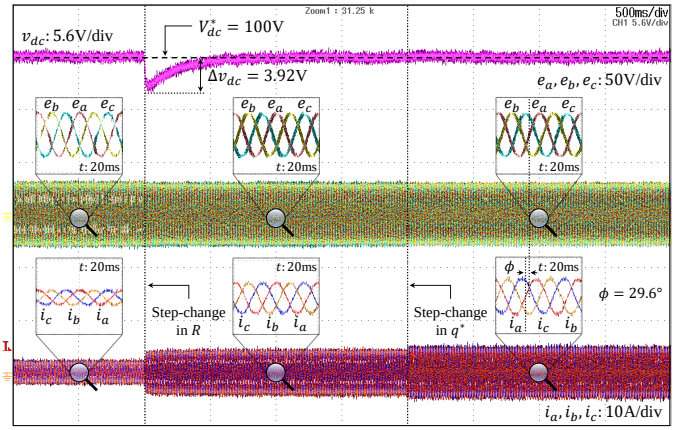

Fig. 8. Experimental result on the converter's performance with the proposed ADR model during a step-response of R and q^*.

C. Case study 3: Effect of unmodelled dynamics and model parameter variation

The converter's performance with the conventional DR control [10] and the proposed ADR control during model parameter uncertainty is shown in Fig. 9a and 9b, respectively. In this study, the load is fixed at $R = 75\Omega$, and the references are set as $V_{dc}^* = 100$V and $q^* = 0$VAR. Until $t = 1$s, the system and model parameters remain the same. Observe that the DR control fails to regulate the v_{dc} to V_{dc}^*. This is because the DR control lacks the loading information R in its model. As a result, a significant $v_{off} = 7.1$V is introduced in v_{dc} during the operation (see Fig. 9a). The v_{off} can be minimized by incorporating the load dynamics into the model. However, such an approach requires an additional current sensor connected through the load for its R estimation. Essentially, the DR model needs to incorporate the discrete-time equation of all the components connected to the dc bus to ensure a minimum v_{off}. Conversely, the proposed ADR control is observed to regulate the v_{dc} to V_{dc}^* without the need for R estimation (see Fig. 9b). The term A in the proposed ADR model provides necessary adjustments to v_{dc}^* based on the accumulated dc bus voltage error over time. As a result, the A compensates for any unmodelled dynamics in the model and ensures a dynamic convergence of v_{dc} to V_{dc}^* during the operation.

At $t = 1$s, a 10% variation is introduced to the parameter C_{dc} as a system non-ideality. The v_{off} is observed to increase for the DR control (see Fig. 9a). This is because the C_{dc} variation directly affects the p_{dc}^* generated for the v_{dc} regulation (see (5)). As a result, the RMS value of the grid currents I_{RMS} is reduced to 2.41A and the v_{dc} settles to 92.2V (Fig. 9a). Meanwhile, the proposed ADR model is observed to regulate the v_{dc} to V_{dc}^* even with a 10% variation in the C_{dc} (see Fig. 9b). Although a dip of $\Delta v_{dc} = 1.3$V is observed in v_{dc} during the transient, A corrects the v_{dc} by providing necessary adjustments to v_{dc}^* through N_L. As a result, the v_{dc} smoothly converges back to V_{dc}^*. Similarly, a 20%, 30%, and 40% variation in C_{dc} is introduced at $t = 2.0$s, $t = 3.0$s, and $t = 4.0$s, respectively. The I_{RMS} for DR control is observed to reduce with the increase in C_{dc} uncertainty. As a result, the v_{off} increases considerably during huge model parameter variations. On the contrary, the proposed ADR control effectively handles the model parameter uncertainty and regulates the v_{dc} to V_{dc}^* throughout the operation (Fig. 9b).

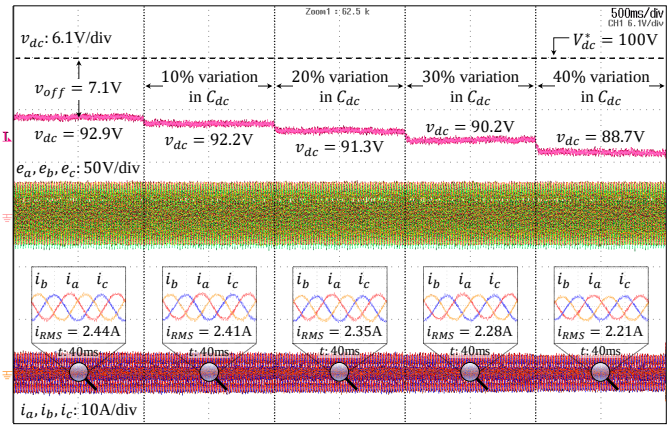

(a)

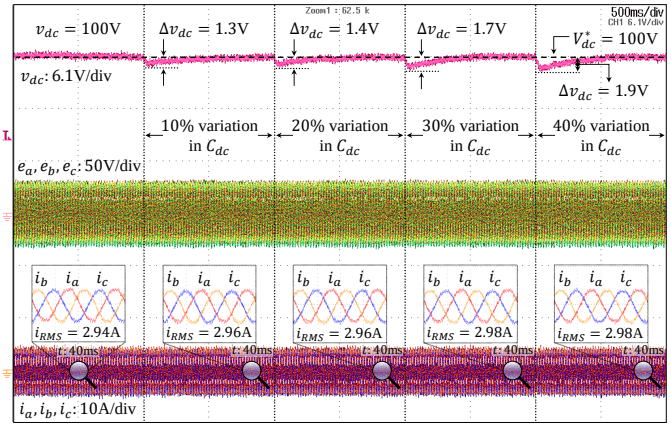

(b)

Fig. 9. Experimental result on the converter's operation under model parameter uncertainty and unmodelled dynamics using, (a) conventional DR model [10], and (b) the proposed ADR model.

D. Case study 4: Effect of sensor imperfections

The experimental result comparing the performance of the proposed ADR with the DR model under sensor imperfection is shown in Fig. 10. In this study, the references are set as $V_{dc}^* = 100$V and $q^* = 0$VAR. A 20% variation in the grid current sensor readings is introduced as a system non-ideality. Until $t = 2.5$s, the conventional DR model generates the v_{dc}^*. Observe that the v_{dc} fails to attain 100V and instead settles at 91.9V. Such steady-state error of $v_{off} = 8.1$V in v_{dc} is significant and can affect the operation of loads connected across the dc bus. The proposed ADR model is activated at $t = 2.5$s. The v_{dc} exhibits a smooth convergence to 100V by eliminating the prevailing v_{off}. This is because the $\frac{A}{N_L}$ of the proposed ADR model is designed to provide necessary adjustments to v_{dc}^* to eliminate the v_{off}. In brief, the proposed ADR control ensures a smooth convergence of v_{dc} to V_{dc}^* during sensor imperfection.

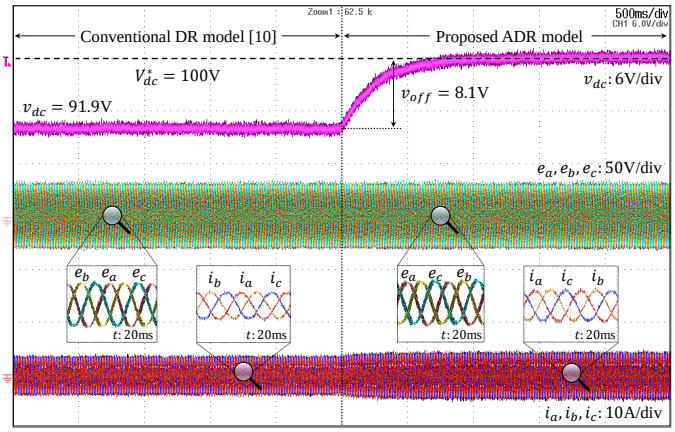

Fig. 10. Experimental result on comparing the performance of proposed ADR model with the DR model during sensor imperfection.

E. Case study 5: Comparison with PI controller

In this section, the effect of step-change in the converter's operating point on its dynamics for a traditional PI controller is studied and compared with the proposed ADR model. To have a fair comparison, the K_p and K_i of the PI controller are designed for the values of $\zeta = 2.5$ and $\omega_n = 20$rad/s, which was considered to obtain parameters N_R and N_L of the ADR model as discussed in Section IV-C. On substituting $\zeta = 2.5$, $\omega_n = 20$rad/s, $V_{dc}^* = 100$V and $R = 10\Omega$ in (23), the parameters K_p and K_i are obtained as 2 and 88, respectively. The experimental result demonstrating the performance of the designed PI controller on the converter operating with $V_{dc}^* = 100$V and load settings: $R = 100\Omega$ and $R = \infty$ is shown in Fig. 11a. Observe that during the step-response at $t = 0.2$s, the dc bus voltage overshoots to 112.6V and possesses an under-damped response even though $\zeta = 2.5$ was selected for the design of gain parameters. This is because the converter operates at a different point ($R = 100\Omega$) compared to the one considered while designing the PI controller ($R = 10\Omega$). The designed PI controller guarantees the desired dc bus voltage response of $\zeta = 2.5$ only if the dc bus load is $R = 10\Omega$. At $t = 1$s, the load is disconnected from the dc bus ($R = \infty$). Observe that the dc bus voltage exhibits an undesirable oscillation with an overshoot of 20.9V during the step-change. To understand this behaviour, the effect of the converter's operating point on the ζ is studied and shown in Fig. 12. Observe that the nature of the dc bus voltage response varies with the converter's operating point for a PI controller. As the loading in the dc bus decreases i.e., R increases, the ζ declines significantly and falls less than 1. Hence, the converter exhibits an oscillatory dc bus voltage response with overshoot when the load across the dc bus is $R = 100\Omega$ ($\zeta = 0.45$) and $R = \infty$ ($\zeta = 0.22$).

The experimental result demonstrating the performance of the converter using the ADR model set at $V_{dc}^* = 100$V with $R = 100\Omega$ and $R = \infty$ is shown in Fig. 11b. Observe that the ADR model exhibits the desired dc bus voltage response ($\zeta = 2.5$) even when the converter's operating point changes (see Fig. 12). This is because the parameters N_R, N_L, and V_e designed for the ADR model are independent of the converter's operating point. Unlike PI controllers, the ADR model ensures the desired dc bus voltage response of $\zeta = 2.5$ for all operating points.

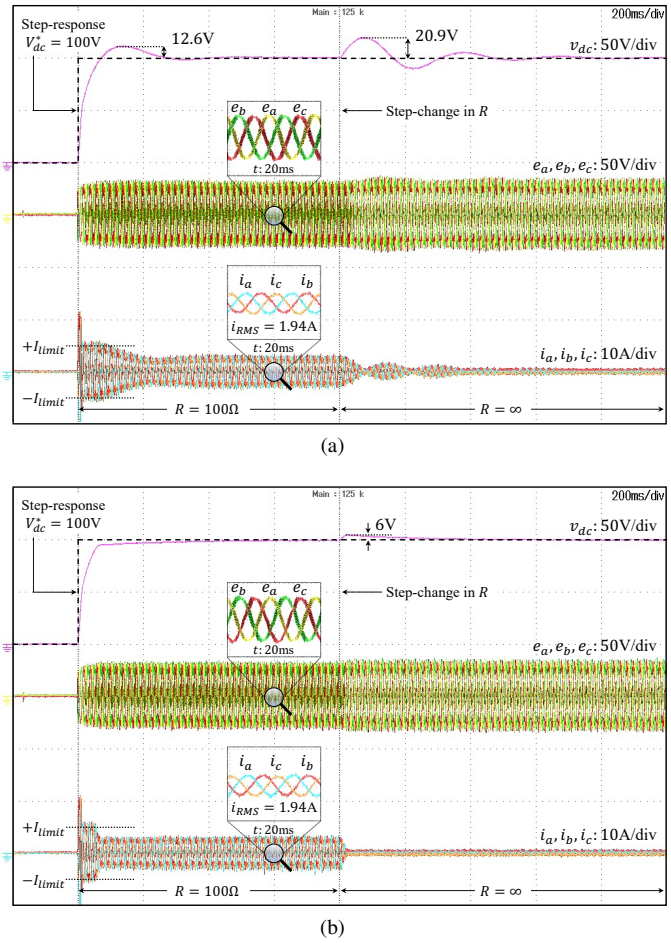

Fig. 11. Experimental result on the converter's performance during a step-change in its operating point when equipped with (a) traditional PI controller, and (b) the proposed ADR model.

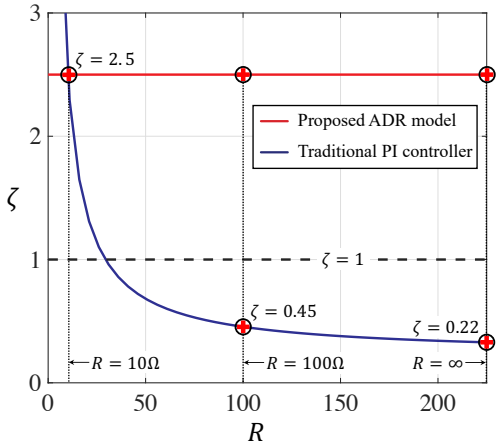

Fig. 12. Effect of converter's operating point on ζ for the proposed ADR model: $N_R = 200$, $N_L = 10^6$, $V_e = 0.1V_{dc}^*$; and traditional PI controller: $K_p = 2$, $K_i = 88$.

VII. Conclusion

An ADR control for the power converters in microgrid was proposed. Unlike conventional methods, the proposed

method utilized a discrete-time model that was easy to design and implement in a digital control platform. Compared to the conventional DR model, the proposed model was capable of handling non-idealities in the system such as the sensor calibration errors/imperfections, unmodeled dynamics, model parameter variations without compromising the overall converter's performance. In addition, the proposed technique does not require an accurate model with all system dynamics incorporated and/or additional dc side current sensor. A theoretical foundation of the proposed ADR model was derived to demonstrate the effect of its parameters on the converter response, and a simple three-step design procedure was developed to obtain the optimal control parameters. The parameter N_R and N_L was selected such that $\zeta > 1$, while V_e was decided based on the PO design limit of the dc bus voltage. Unlike PI controllers, the design of the proposed ADR model was independent of the loading and voltage reference value. The experimental results of the proposed ADR model with FCS-MPC, out performed the conventional DR model by demonstrating an effective dynamic convergence of the dc bus voltage to its reference under system non-idealities. In addition, the proposed ADR model always exhibited the desired dc bus voltage response compared to the PI controller during a step-change in the converter's operating point.

APPENDIX A
DERIVATION FOR $v^*_{dc}(t)$

On substituting the initial conditions: $\frac{dv^*_{dc}(0)}{dt} = 0$, $v^*_{dc}(0) = V^*_{dc} - V_e$, $V^*_{dc}(0) = V^*_{dc} - V_e$ to (11), the $v^*_{dc}(s)$ can be expressed as

$$v^*_{dc}(s) = \frac{\frac{1}{N_R T_s}s + \frac{1}{N_L T_s^2}}{s^2 + \frac{1}{N_R T_s}s + \frac{1}{N_L T_s^2}} V^*_{dc}(s) + \frac{s(V^*_{dc} - V_e)}{s^2 + \frac{1}{N_R T_s}s + \frac{1}{N_L T_s^2}}. \quad (24)$$

Applying step-response on (24), i.e., assigning $V^*_{dc}(s) = \frac{V^*_{dc}}{s}$, the $v^*_{dc}(s)$ can be obtained in terms of V^*_{dc} and V_e as

$$v^*_{dc}(s) = \frac{\frac{1}{N_R T_s} + \frac{1}{sN_L T_s^2}}{s^2 + \frac{1}{N_R T_s}s + \frac{1}{N_L T_s^2}} V^*_{dc} + \frac{s(V^*_{dc} - V_e)}{s^2 + \frac{1}{N_R T_s}s + \frac{1}{N_L T_s^2}}. \quad (25)$$

Through further simplification, (25) can be rewritten as

$$v^*_{dc}(s) = \frac{\left(s + \frac{1}{N_R T_s} + \frac{1}{sN_L T_s^2}\right) V^*_{dc} - sV_e}{s^2 + \frac{1}{N_R T_s}s + \frac{1}{N_L T_s^2}} \quad (26)$$

For simplicity, the expression in the denominator of (26) can be written as

$$s^2 + \frac{1}{N_R T_s}s + \frac{1}{N_L T_s^2} = \left(s + \frac{0.5}{N_R T_s}\right)^2 + \left(\frac{x}{\zeta}\sqrt{1-\zeta^2}\right)^2. \quad (27)$$

From (16) and (27), (26) can be simplified as

$$v^*_{dc}(s) = \frac{\left(s + 2x + \frac{x^2+y^2}{s}\right) V^*_{dc} - sV_e}{(s+x)^2 + y^2}. \quad (28)$$

Through partial fraction decomposition, (28) can be further simplified as

$$v^*_{dc}(s) = \frac{1}{s}V^*_{dc} - \frac{s}{(s+x)^2 + y^2}V_e. \quad (29)$$

Observe that $y = 0$ for $\zeta = 1$ (16). Thus, (29) can be decomposed into two expressions based on ζ as

$$v^*_{dc}(s) = \begin{cases} \frac{1}{s}V^*_{dc} - \frac{s}{(s+x)^2+y^2}V_e, & \text{for } \zeta \neq 1 \\ \frac{1}{s}V^*_{dc} - \frac{s}{(s+x)^2}V_e, & \text{for } \zeta = 1 \end{cases}. \quad (30)$$

Finally, applying the inverse Laplace transform on (30), the expression for $v^*_{dc}(t)$ presented in (15) is obtained.

APPENDIX B
DERIVATION FOR t_m

The expression for t_m is obtained by differentiating (15) with respect to time and equating to zero. The differentiation of (15) with respect to t is expressed as

$$\frac{dv^*_{dc}(t)}{dt} = \begin{cases} V_e\left(2x\cos yt - \left(\frac{x^2-y^2}{y}\right)\sin yt\right)e^{-xt}, & \text{for } \zeta \neq 1 \\ V_e x\left(2 - xt\right)e^{-xt}, & \text{for } \zeta = 1 \end{cases} \quad (31)$$

On setting $t = t_m$ and $\frac{dv^*_{dc}(t_m)}{dt} = 0$, the expressions in (31) can be written as

$$\tan yt_m = \frac{2xy}{x^2 - y^2}, \quad \text{for } \zeta \neq 1, \quad (32)$$

$$xt_m = 2, \quad \text{for } \zeta = 1. \quad (33)$$

Unlike (33), the t_m in (32) has infinite possible solutions due to the presence of a tangent function. Thus, the general solution of (32) can be expressed as

$$t_m = \frac{n\pi}{y} + \frac{1}{y}\tan^{-1}\left(\frac{2xy}{x^2 - y^2}\right), \text{ where } n \in \mathbb{Z}. \quad (34)$$

Since the first peak of the response is always maximum (see Fig. 3), the t_m is obtained by setting $n = 0$. However, when $x < y$, the obtained t_m becomes negative. Such solution is undefined as t_m should always be positive. Therefore, a positive t_m is obtained by setting $n = 1$ when $x < y$. From (16), the expression $x < y$ can be written as

$$x < \frac{x}{\zeta}\sqrt{1-\zeta^2}. \quad (35)$$

On simplifying (35), the range of ζ for $x < y$ is determined as

$$\zeta < 1/\sqrt{2}. \quad (36)$$

Thus, $n = 1$ is considered for $\zeta < 1/\sqrt{2}$ to obtain a positive t_m. From (33), (34), and (36), the expression for t_m under different ζ is obtained as presented in (18).

REFERENCES

[1] S. Devassy and B. Singh, "Design and Performance Analysis of Three-Phase Solar PV Integrated UPQC," *IEEE Trans. Ind. Appl.*, vol. 54, DOI 10.1109/ICPES.2016.7584022, no. 1, pp. 73–81, Feb. 2018.

[2] S. K. Kollimalla, M. K. Mishra, A. Ukil and H. B. Gooi, "DC Grid Voltage Regulation Using New HESS Control Strategy," *IEEE Trans. Sustain. Energy*, vol. 8, DOI 10.1109/TSTE.2016.2619759, no. 2, pp. 772-781, Apr. 2017.

[3] A. Merabet, K. Tawfique Ahmed, H. Ibrahim, R. Beguenane and A. M. Y. M. Ghias, "Energy Management and Control System for Laboratory Scale Microgrid Based Wind-PV-Battery," *IEEE Trans. Sustain. Energy*, vol. 8, DOI 10.1109/TSTE.2016.2587828, no. 1, pp. 145-154, Jan. 2017.

[4] A. Parida, S. Choudhury and D. Chatterjee, "Microgrid Based Hybrid Energy Co-Operative for Grid-Isolated Remote Rural Village Power Supply for East Coast Zone of India," *IEEE Trans. Sustain. Energy*, vol. 9, DOI 10.1109/TSTE.2017.2782007, no. 3, pp. 1375-1383, Jul. 2018.

[5] Z. Yi, W. Dong and A. H. Etemadi, "A Unified Control and Power Management Scheme for PV-Battery-Based Hybrid Microgrids for Both Grid-Connected and Islanded Modes," *IEEE Trans. Smart Grid*, vol. 9, DOI 10.1109/TSG.2017.2700332, no. 6, pp. 5975-5985, Nov. 2018.

[6] P. Cortes, M. P. Kazmierkowski, R. M. Kennel, D. E. Quevedo and J. Rodriguez, "Predictive Control in Power Electronics and Drives," *IEEE Trans. Ind. Electron.*, vol. 55, DOI 10.1109/TIE.2008.2007480, no. 12, pp. 4312-4324, Dec. 2008.

[7] P. Cortes, J. Rodriguez, P. Antoniewicz and M. Kazmierkowski, "Direct Power Control of an AFE Using Predictive Control," *IEEE Trans. Power Electron.*, vol. 23, DOI 10.1109/TPEL.2008.2002065, no. 5, pp. 2516-2523, Sep. 2008.

[8] P. Acuña et al, "A Single-Objective Predictive Control Method for a Multivariable Single-Phase Three-Level NPC Converter-Based Active Power Filter," *IEEE Trans. Ind. Electron.*, vol. 62, DOI 10.1109/TIE.2015.2393556, no. 7, pp. 4598-4607, Jul. 2015.

[9] P. Falkowski and A. Sikorski, "Finite Control Set Model Predictive Control for Grid-Connected AC–DC Converters With LCL Filter," *IEEE Trans. Ind. Electron.*, vol. 65, DOI 10.1109/TIE.2017.2750627, no. 4, pp. 2844-2852, Apr. 2018.

[10] D. E. Quevedo, R. P. Aguilera, M. A. Perez, P. Cortes and R. Lizana, "Model Predictive Control of an AFE Rectifier With Dynamic References," *IEEE Trans. Power Electron.*, vol. 27, DOI 10.1109/TPEL.2011.2179672, no. 7, pp. 3128-3136, Jul. 2012.

[11] P. Acuna et al., "Cascade-Free Model Predictive Control for Single-Phase Grid-Connected Power Converters," *IEEE Trans. Ind. Electron.*, vol. 64, DOI 10.1109/TIE.2016.2599478, no. 1, pp. 285-294, Jan. 2017.

[12] V. Jayan and A. Ghias, "Finite Control Set Model Predictive Control of a Nine Switch Dual Output Converter as a Power Quality Conditioner," *IEEE Int. Conf. Ind. Tech.*, 2019, DOI 10.1109/ICIT.2019.8755152, pp. 1241-1246.

[13] V. Jayan, A. Ghias and A. Merabet, "Modeling and Control of Three-level Bi-directional Flying Capacitor DC-DC converter in DC microgrid," *IECON 2019 - 45th Annual Conf. IEEE Ind. Electron. Soc.*, 2019, DOI 10.1109/IECON.2019.8926699, pp. 4113-4118.

[14] V. Jayan and A. Ghias, "Operation and Control of Five-level Bi-directional Flying Capacitor DC-DC converter in DC microgrid," *IEEE 4th Int. Future Energy Electron. Conf. (IFEEC)*, 2019, DOI 10.1109/IFEEC47410.2019.9015201, pp. 1-6.

[15] V. Jayan, A. Ghias and A. Merabet, "Fixed Frequency Model Predictive Control of Three-level Bi-directional Flying Capacitor DC-DC converter in DC microgrid," *IECON 2019 - 45th Annual Conf. IEEE Ind. Electron. Soc.*, 2019, DOI 10.1109/IECON.2019.8927435, pp. 3343-3348.

[16] V. Jayan and A. Ghias, "Fixed Frequency Model Predictive Control of Five-level Bi-directional Flying Capacitor DC-DC converter in DC microgrid," *IEEE 4th Int. Future Energy Electron. Conf. (IFEEC)*, 2019, DOI 10.1109/IFEEC47410.2019.9015054, pp. 1-6.

[17] Y. Shan, J. Hu, Z. Li and J. M. Guerrero, "A Model Predictive Control for Renewable Energy Based AC Microgrids Without Any PID Regulators," *IEEE Trans. Power Electron.*, vol. 33, DOI 10.1109/TPEL.2018.2822314, no. 11, pp. 9122-9126, Nov. 2018.

[18] Y. Shan, J. Hu, K. W. Chan, Q. Fu and J. M. Guerrero, "Model Predictive Control of Bidirectional DC–DC Converters and AC/DC Interlinking Converters—A New Control Method for PV-Wind-Battery Microgrids," *IEEE Trans. Sustain. Energy*, vol. 10, DOI 10.1109/TSTE.2018.2873390, no. 4, pp. 1823-1833, Oct. 2019.

[19] Y. Shan, J. Hu and J. M. Guerrero, "A Model Predictive Power Control Method for PV and Energy Storage Systems With Voltage Support Capability," *IEEE Trans. Smart Grid*, vol. 11, DOI 10.1109/TSG.2019.2929751, no. 2, pp. 1018-1029, Mar. 2020.

[20] Y. Shan, J. Hu, M. Liu, J. Zhu and J. M. Guerrero, "Model Predictive Voltage and Power Control of Islanded PV-Battery Microgrids With Washout-Filter-Based Power Sharing Strategy," *IEEE Trans. Power Electron.*, vol. 35, DOI 10.1109/TPEL.2019.2930182, no. 2, pp. 1227-1238, Feb. 2020.

[21] A. S. Samosir and A. H. M. Yatim, "Implementation of Dynamic Evolution Control of Bidirectional DC–DC Converter for Interfacing Ultracapacitor Energy Storage to Fuel-Cell System," *IEEE Trans. Ind. Electron.*, vol. 57, DOI 10.1109/TIE.2009.2039458, no. 10, pp. 3468-3473, Oct. 2010.

[22] U. Manandhar, B. Wang, A. Ukil and H. B. Gooi, "Dynamic evolution control based power sharing method for hybrid energy storage system," *IET Power Electron.*, vol. 12, DOI 10.1049/iet-pel.2018.5462, no. 2, pp. 276-283, Feb. 2019.

[23] Y. Yang, S. Tan and S. Y. R. Hui, "Adaptive Reference Model Predictive Control With Improved Performance for Voltage-Source Inverters," *IEEE Trans. Control Syst. Tech.*, vol. 26, DOI 10.1109/TCST.2017.2670529, no. 2, pp. 724-731, Mar. 2018.

[24] M. Norambuena, P. Lezana and J. Rodriguez, "A Method to Eliminate Steady-State Error of Model Predictive Control in Power Electronics," *IEEE J. Emerg. Sel. Topics Power Electron.*, vol. 7, DOI 10.1109/JESTPE.2019.2894993, no. 4, pp. 2525-2530, Dec. 2019.

[25] Jose Rodriguez, Patricio Cortes, "Predictive Control of a Three-Phase Inverter," *Predictive Control of Power Converters and Electrical Drives*, IEEE, DOI 10.1002/9781119941446.ch4, 2012, pp. 41-63.

[26] Hirofumi Akagi, Edson Hirokazu Watanabe, Mauricio Aredes, "The Instantaneous Power Theory," *Instantaneous Power Theory and Applications to Power Conditioning*, IEEE, DOI 10.1002/9781119307181.ch3, 2017, pp. 37-109.

[27] Tony Roskilly, Rikard Mikalsen, "System Transfer Functions," *Marine Systems Identification, Modeling and Control*, DOI 10.1016/B978-0-08-099996-8.00003-3, 2015, pp. 37-67.

Vijesh Jayan (Student Member, IEEE) received the B.Tech. degree in electrical and electronics engineering from the National Institute of Technology Puducherry, Karaikal, India, in 2016. He is currently working towards the Ph.D. degree in power engineering with the School of Electrical and Electronic Engineering, Nanyang Technological University, Singapore.

From 2016 to 2018, he was a Technical Trainee under Nuclear Power division in Lloyd's Register Energy Pvt. Ltd., Mumbai, India. His research interests include power converter topologies, model predictive control, renewable energy systems, and power quality.

Amer M. Y. M. Ghias (Senior Member, IEEE) received the B. Sc. degree in electrical engineering from Saint Cloud State University, USA, in 2001, the M. Eng. degree in telecommunications from University of Limerick, Ireland, in 2006, and the Ph.D. degree in electrical engineering from the University of New South Wales (UNSW), Australia, in 2014.

From February 2002 to July 2009, he had held various positions such as Electrical Engineer, Project Engineer, and Project Manager, while working with the top companies in Kuwait. He was with UNSW during 2014-2015, and the University of Sharjah, United Arab Emirates, during 2015-2018. In 2018, he joined the Nanyang Technological University as an Assistant professor. He is also a Cluster Director (Power Electronics and the Energy Management) for Energy Research Institute @ NTU (ERI@N), Singapore. His research interests include model predictive control, hybrid energy storage, renewable energy sources, multi-phase drives, new multilevel converters, and advanced modulations for the multilevel converter.

Dr. Amer is an Editor for *IET Power Electronics*.

Josep M. Guerrero (Fellow, IEEE) received the B.S. degree in telecommunications engineering, the M.S. degree in electronics engineering, and the Ph.D. degree in power electronics from the Technical University of Catalonia, Barcelona, Spain, in 1997, 2000, and 2003, respectively. Since 2011, he has been a Full Professor with the Department of Energy Technology, Aalborg University, Aalborg, Denmark, where he is responsible for the Microgrid Research Program. Since 2014, he has been a Chair Professor with Shandong University, Jinan, China. Since 2015, he has been a Distinguished Guest Professor with Hunan University, Changsha, China. Since 2016, he has been a Visiting Professor Fellow with Aston University, Birmingham, U.K., and a Guest Professor with Nanjing University of Posts and Telecommunications, Nanjing, China. In 2019, he became Villum Investigator. He has published more than 500 journal articles in the fields of microgrids and renewable energy systems, which are cited more than 30 000 times. His research interests include different microgrid aspects, including power electronics, distributed energy storage systems, hierarchical and cooperative control, energy management systems, smart metering, and the Internet of Things for ac/dc microgrid clusters, and islanded minigrids. His recent specific research interests include maritime microgrids for electrical ships, vessels, ferries, and seaports. He was elevated as an IEEE Fellow for his contributions on distributed power systems and microgrids, in 2015. He received the Best Paper Award of the IEEE Transactions on Energy Conversion for the period 2014–2015 and the Best Paper Prize of the IEEE Power and Energy Society (PES), in 2015. He also received the Best Paper Award of the Journal of Power Electronics, in 2016. During five consecutive years, from 2014 to 2018, he was awarded by Clarivate Analytics (former Thomson Reuters) as a Highly Cited Researcher. He is an Associate Editor for a number of the IEEE Transactions

Adel Merabet (Senior Member, IEEE) received the Ph.D. degree in engineering from the University of Québec at Chicoutimi, Canada in 2007. He joined Saint Mary's University in 2009 and currently he is an Associate Professor with the Division of Engineering. In 2016–2017, he was a Visiting Academic with the Department of Sustainable and Renewable Energy Engineering, University of Sharjah, Sharjah, UAE. In 2019, he was the recipient of the Tan Chin Tuan Exchange Fellowship in Engineering from Nanyang Technological University in Singapore. In 2021, he was Visiting Research Scientist at Khalifa University, Abu Dhabi, UAE. His research interests include renewable (wind-solar) energy conversion systems, energy management, advanced control, electric drives, artificial intelligence, and smart grid.